

## P2.1 Improving numerical forecasting of the wind by using LIDAR data in the Local Analysis and Prediction System (LAPS)

Svenja Koos  
University of Hannover, Hannover, Germany

C.S. Lau  
Chinese University of Hong Kong, Hong Kong, China

P.W. Chan \*  
Hong Kong Observatory, Hong Kong, China

### 1. INTRODUCTION

The Hong Kong International Airport (HKIA) is situated in an area of complex terrain. To its south is the mountainous Lantau Island (Figure 1) with peaks rising to about 1000 m AMSL with valleys as low as 400 m in between. Terrain disruption of the airflow poses a great challenge in the short-term forecasting of the wind at the airport, which is an important element in the aviation weather services. The airflow disturbances could also bring about low-level windshear and turbulence to the landing/departing aircraft at HKIA.

The low-level winds at HKIA have been forecast with some success in selected cases of terrain-disrupted airflow by using the Regional Atmospheric Modelling System (RAMS) version 4.4 (Cotton et al. 2003). In Szeto and Chan (2006), a regime diagram was constructed for the occurrence of mountain wake downstream of Lantau Island in the prevailing east to southeasterly airstream in the spring. Chan (2006) also conducted super-high resolution of numerical simulation (with a horizontal grid of 50 m) to study the airflow disturbances in the airport area in spring-time easterly condition. In these studies, the initial analyses of the atmospheric condition were obtained using the synoptic weather data as well as the observations within Hong Kong such as the measurements from the automatic weather stations (AWS) and wind profilers.

For monitoring the winds at HKIA, the Hong Kong Observatory (HKO) operates two Doppler Light Detection And Ranging (LIDAR) systems at the airport. The LIDARs provide radial velocities up to a range of 10 km in high temporal (every 6 minutes) and spatial (about 1 degree in azimuth and 105 m in range) resolutions for the surveillance scans (also known as the Plan Position Indicator, or PPI, scans). In this paper, the impact of the LIDAR data on the numerical wind forecasting at the airport area will be studied. As a first step, only the LIDAR near the centre of the airfield, viz. situated at about 50 m AMSL on top of the Air Traffic Control Complex at HKIA would be considered (location in Figure 1).

RAMS requires the input of the full horizontal wind vectors, which are not directly measured by the LIDAR. As such, an analysis package of the meteorological field is required. The Local Analysis

and Prediction System (LAPS) is employed to assimilate the LIDAR observations as well as other measurements within the Hong Kong territory and generate the initial meteorological field. This field is then ingested into RAMS for short-term forecasting of the wind (in the next couple of hours) and the results are verified by comparing with the LIDAR observations at the later times. The features of LAPS and RAMS as employed in this study are briefly summarized in Section 2. A case study is conducted on the quality of the forecast wind field, namely, a spring-time easterly wind event. It is described in Section 3. The conclusions of the paper are drawn in Section 4.

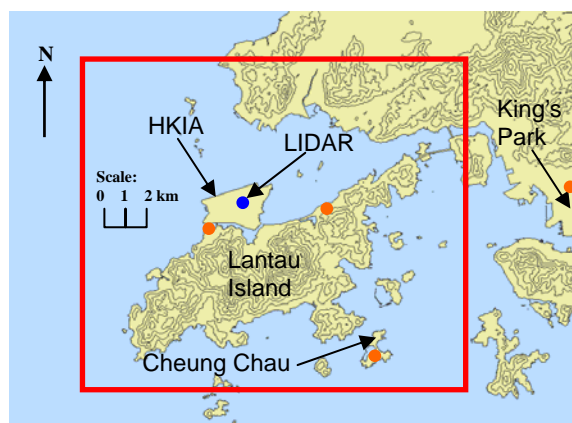


Figure 1 The analysis domain of LAPS in this paper, as indicated by the red rectangle. The terrain contours are in 100 m. The wind profilers are shown as orange dots.

### 2. LAPS AND RAMS

A description of LAPS could be found in McGinley et al. (1991). The analysis domain employed in this study is shown in Figure 1, which includes the seas surrounding HKIA on the three sides, the Lantau Island and the area just upstream of this Island in easterly to southeasterly wind. It contains the 10-km measurement range covered by the LIDAR at the middle of the airfield.

To resolve the complex terrain in the airport area, the terrain data at 100 m resolution for Hong Kong are adopted in LAPS. The weather data analysis grid has a size of 150 m. The analysis domain has 200 grids in the east-west direction and 168 grids in the north-south direction. There are 30 levels in the vertical. Between 1000 and 900 hPa, the vertical resolution is 10 hPa. The resolution becomes 50 hPa aloft, between 900 and 100 hPa.

\* Corresponding author address: P.W. Chan, Hong Kong Observatory, 134A Nathan Road, Hong Kong email: [pwchan@hko.gov.hk](mailto:pwchan@hko.gov.hk)

The three PPI scans of the LIDAR are ingested into LAPS, namely, at the elevation angles of 0, 1 and 4.5 degrees. In addition, the analysis makes use of the conventional data sources such as the surface AWS network, wind profilers, radio acoustic sounding system (RASS) and weather radars. The balanced meteorological field is obtained by enforcing dynamical consistency between the wind and pressure fields. In this paper, only the LAPS-analyzed wind field is input into RAMS for forecasting.

The setup of RAMS for wind forecasting at HKIA could be found in Szeto and Chan (1996). The domains of the numerical simulation are shown in Figure 2. Nesting runs with resolutions of 4 km (grid 1), 800 m (grid 2) and 200 m (grid 3) are conducted. Two-way interactive nesting is adopted. The innermost domain (grid 3) is centred at the airport area, similar to the LAPS analysis domain as shown in Figure 1. The LAPS analysis data are used to construct the initial fields of grids 1 and 2 only. Apart from the LAPS analysis, no other observations are considered in the initialization of RAMS. The RAMS is nested with the Operational Regional Spectral Model (ORSM) of HKO as the outer model.

Concerning the choice of model physics, the only thing which is different from Szeto and Chan (2006) is the turbulence parameterization scheme. Chan (2006) found that, among the turbulence schemes available in RAMS, Deardorff (1980) scheme appeared to have the best performance in reproducing the small-scale wind fluctuations in the airport area arising from terrain disruption. As a result, it is employed in grid 3 whereas Mellor and Yamada (1982) scheme is still used in the other two grids due to the coarser horizontal resolutions.

### 3. CASE STUDY

The springtime easterly wind case considered in Chan (2006) is studied in this paper again. It occurred in the early morning of 2 February 2006. The LAPS analysis is carried out at 18 UTC, 1 February 2006 (Hong Kong time = UTC + 8 hours). Synoptic upper-air observations are not available at this time and the winds in the boundary layer only come from the LIDAR and the wind profiler observations (locations of the wind profilers in Figure 1). Due to the high spatial density, the LIDAR's radial velocities are believed to overwhelm the analysis of the horizontal wind field in the first few hundred metres in the troposphere.

To see the effect of LIDAR data in the analysis, the balanced wind fields from LAPS at 1000 hPa (about 120 m AMSL, the lowest pressure level apart from the surface available from LAPS) with and without the use of LIDAR winds are shown in Figure 3. Also included in this figure are the LIDAR observations employed in the analysis of this pressure level and the plot of LIDAR radial velocity at 0-degree PPI scan at the same time for comparison. Without the use of LIDAR data, the analyzed wind field (Figure 3a) is found to have the following discrepancies compared to the actual observations (Figure 3(d)): (i) the mountain wake downstream of Lantau Island is

larger in extent, and (ii) the flow emerging from the gaps to the east of HKIA has larger southerly component. The inclusion of LIDAR data in the analysis helps remove these discrepancies (Figure 3(b) and (c)). Moreover, the upstream easterly jet is resolved to the east of Lantau Island. Therefore, the inclusion of LIDAR data in the generation of the balanced meteorological field not only affects the winds in the airport area, but also the airflow upstream of Lantau Island over which LIDAR measurements are not available.

In both analysis fields, there are a couple of features that do not appear to be realistic. First of all, a southeasterly jet of 30-40 knots is analyzed at the southwestern part of the domain. There are no observations to support the occurrence of this jet. It may arise due to the limited size of the analysis domain. Secondly, at several gaps as well as the southwestern tip of Lantau Island, the analyzed wind could reach about 60 knots. Again, this near-hurricane force gap/"corner" flow is not supported by observations. Maybe the current setting of LAPS, which has been mainly used for mesoscale analysis, requires further adjustments in handling constrictions/corners in the terrain resolved in much higher spatial resolutions (~150 m). These topics would be considered in future research.

The LAPS analysis with the inclusion of LIDAR data is used to initialize the RAMS run. As the control experiment, RAMS is also run without using the LAPS analysis, but with its own analysis package for all the available observations at 18 UTC, 1 February 2006 excluding the LIDAR data. The forecast wind fields from these two runs valid at 19:40 UTC, 1 February 2006 are shown in Figure 4. In the control experiment, the mountain wake with reversed flow to the west of HKIA is found to be much exaggerated in comparison with the actual LIDAR observations – it has too large spatial extent (Figure 4(c)). Moreover, the easterly jet on the western part of HKIA is weaker. The RAMS forecast as initialized by LIDAR data (Figure 4(d)) is closer to reality (Figure 4(a)), though the reversed flow appears to be a bit too weak to the southwest of the airport.

To see how the differences in the forecast wind fields in the airport area could come about from these two runs, the temperature and wind speed profiles at Cheung Chau (location in Figure 1) in the simulations are plotted in Figure 4 to represent the background thermodynamic and dynamic profiles. For comparison, the wind profiler measurements at about 19:40 UTC, 1 February 2006 are also plotted in Figure 4(b). However, temperature profile is not measured at Cheung Chau at that time. Only the radiosonde data at 00 UTC, 2 February 2006 as obtained at King's Park (location in Figure 1) are employed. In the control experiment, a more or less isothermal layer appears in the lowest 400 m of the boundary layer (Figure 4(e)), which is not observed in reality (Figure 4(b)). The boundary layer jet also has too large vertical extent, appearing between 500 and 1000 m. The near-ground isothermal layer coupled with the easterly jet could bring about the extensive area of mountain wake/reversed flow to the west of HKIA. On the other hand, with the inclusion of LIDAR data in the analysis, the near-ground

isothermal layer does not occur and the altitude of the boundary-layer easterly jet is closer to reality (Figure 4(f)). It is interesting to note that, though only the LAPS-analyzed *wind* field is used to initialize RAMS, improvement of the forecast results could be achieved for the *temperature* profile upstream of Lantau Island, which in turn has a positive impact on the forecasting of terrain-disrupted airflow over HKIA. However, even with the inclusion of LIDAR data in the LAPS analysis, the temperature profile in the analysis field does not reproduce the sharp temperature inversion of about 5 degrees between 700 and 900 m AMSL (Figure 4(b)). The origin of this temperature inversion requires further study.

#### 4. CONCLUSIONS

The application of LIDAR data in the short-term forecasting of the wind at HKIA using a numerical weather prediction model is studied in this paper. The LIDAR's radial velocities are input into LAPS, together with the other weather observations, to produce an initial wind field, which is used to drive three nested runs of RAMS. For the spring-time easterly wind case with a stable boundary layer, the incorporation of LIDAR data in the model initialization is found to have positive impact on the forecasting of the background temperature and wind profiles upstream of Lantau Island. This in turn improves the simulation of terrain-disrupted airflow in the vicinity of HKIA.

Future studies would include the impact of LIDAR data on wind forecasting at HKIA in other weather conditions, such as strong southwest monsoon. The inclusion of LAPS-analyzed temperature and vertical velocity fields would also be considered.

#### References

- Chan, P.W., 2006: Super-high-resolution numerical simulation of atmospheric turbulence in an area of complex terrain. *12<sup>th</sup> Conference on Mountain Meteorology*, American Meteorological Society.
- Cotton, W.R., R.A. Pielke Sr., R.L. Walko, G.E. Liston, C. Tremback, H. Jiang, R.L. McAnelly, J.Y. Harrington, M.E. Nicholls, G.G. Carrio and J.P. McFadden, 2003: RAMS 2001: Current status and future directions. *Meteor. Atmos. Phys.*, **82**, 5-29.
- Deardorff, J.W., 1980: Stratocumulus-capped mixed layers derived from a three-dimensional model. *Bound.-Layer Meteor.*, **18**, 495–527.
- McGinley, J. A., S. C. Albers, and P. A. Stamus, 1991: Validation of a composite convective index as defined by a real-time local analysis system. *Wea. Forecasting*, **6**, 337–356.
- Mellor, G. L., and T. Yamada, 1982: Development of a turbulence closure model for geophysical fluid problems. *Rev. Geophys. Space Phys.*, **20**, 851–875.
- Szeto, K.C., and P.W. Chan, 2006: High resolution numerical modelling of windshear episodes at the Hong Kong International Airport. *12<sup>th</sup> Conference on Aviation, Range, and Aerospace Meteorology*, American Meteorological Society.

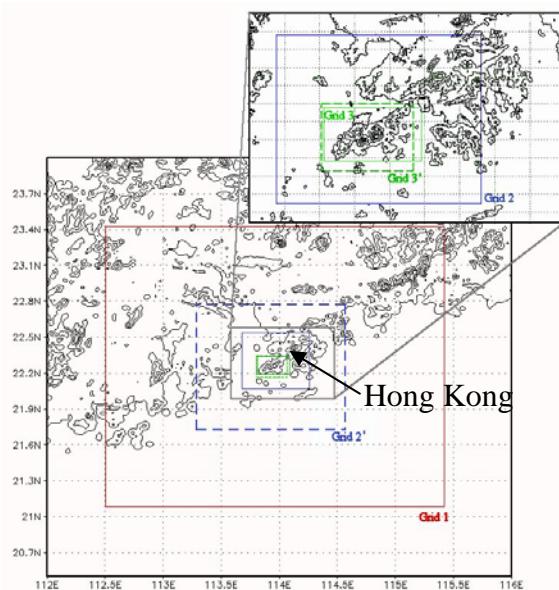
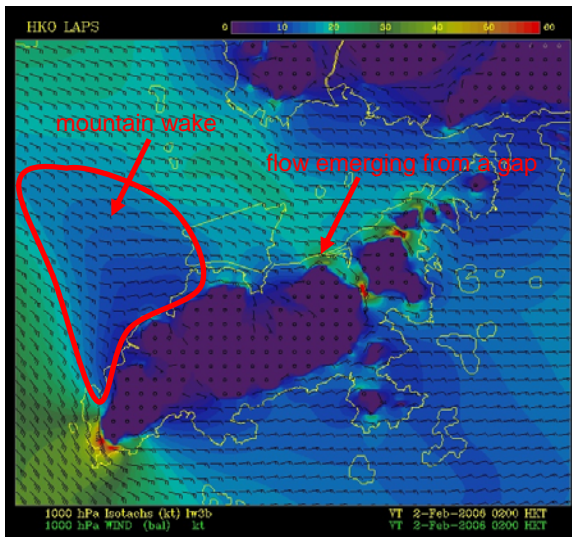
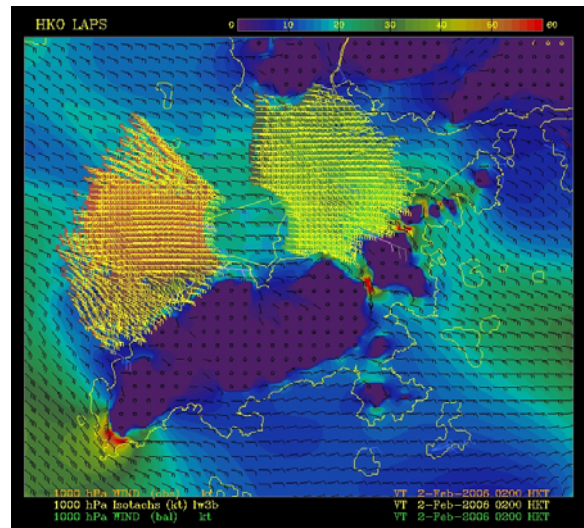


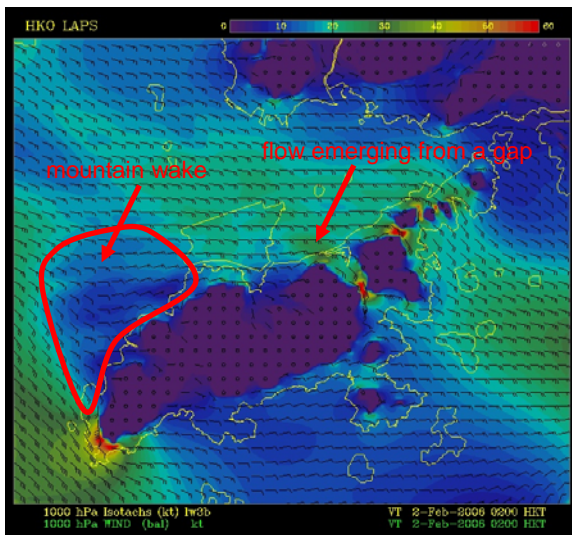
Figure 2 Domains of the nested model grids: solid lines refer to the domains in Grids 1, 2 and 3 of the simulation (reproduced from Szeto and Chan (2006)).



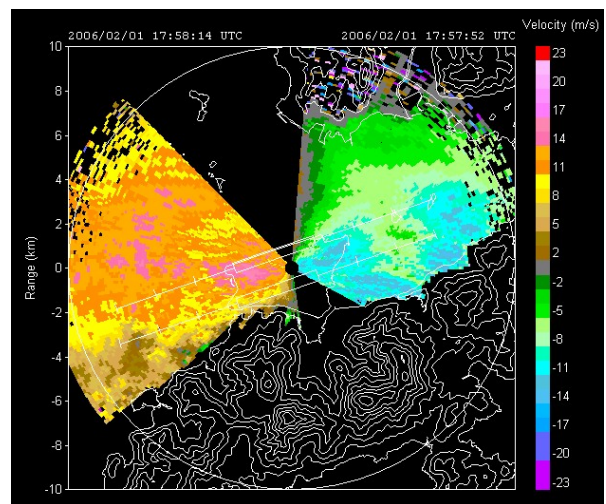
(a)



(b)

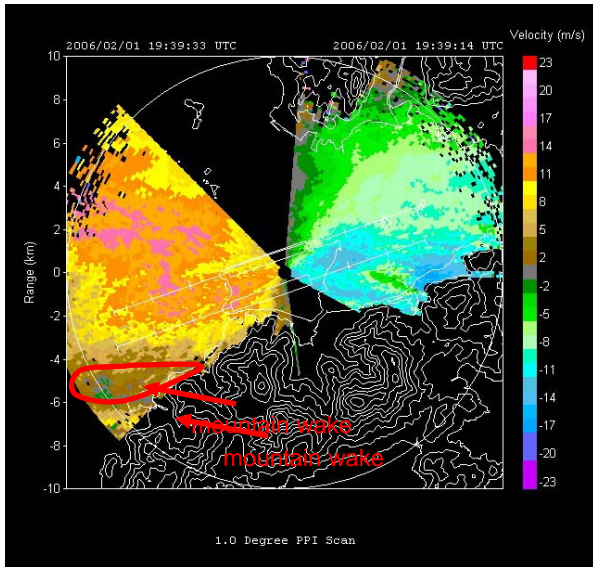


(c)

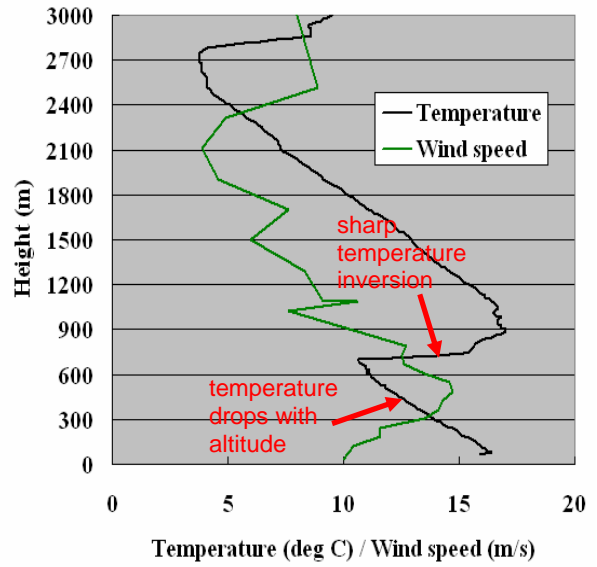


(d)

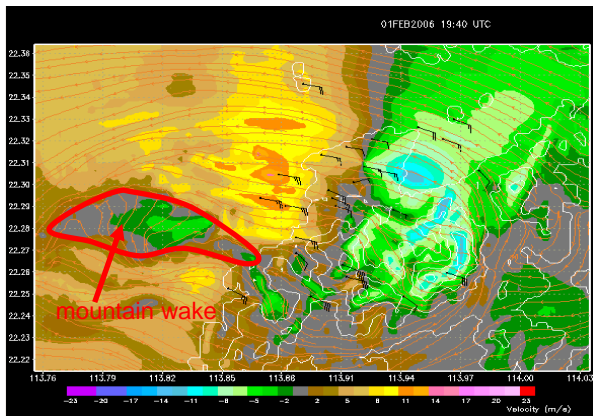
Figure 3 The analyzed wind field at 1000 hPa by LAPS without the use of LIDAR data (a). The distribution of LIDAR data used in the analysis (the affected wind data in the analysis are shown in yellow wind bars) is given in (b). The analyzed wind field with the inclusion of LIDAR data is shown in (c). (d) is the corresponding radial velocity distribution from the LIDAR in 1-degree PPI scan.



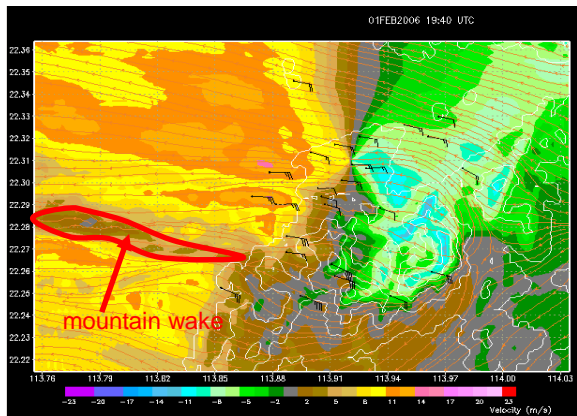
(a)



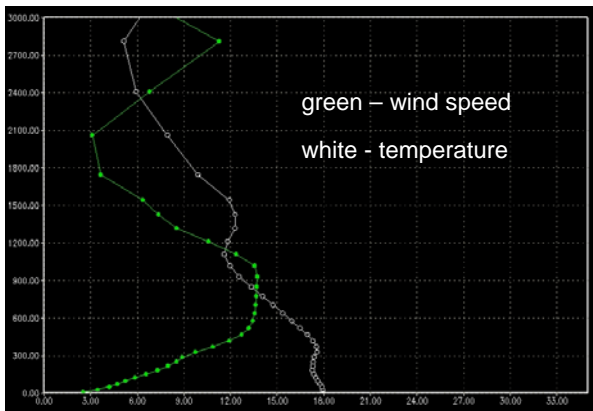
(b)



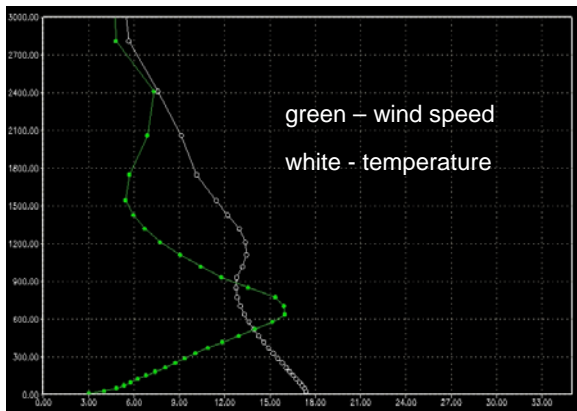
(c)



(d)



(e)



(f)

Figure 4 The radial velocity distribution from the LIDAR in 1-degree PPI scan at 19:39 UTC, 1 February 2006 is shown in (a). (b) gives the temperature and the wind speed profiles measured at a location upstream of Lantau Island. (c) and (e) are the RAMS simulation results without the use of LIDAR data for LIDAR radial velocity at 50 m AMSL and the temperature/wind speed profiles at an upstream location respectively. (d) and (f) are the corresponding simulation results with the inclusion of LIDAR data.